available at www.sciencedirect.com
journal homepage: www.europeanurology.com

European Association of Urology

Platinum Priority – Surgery in Motion

Editorial by Morgan Pokorny ans John Yaxley on pp. 515–516 of this issue

Three-dimensional Elastic Augmented-reality Robot-assisted Radical Prostatectomy Using Hyperaccuracy Three-dimensional Reconstruction Technology: A Step Further in the Identification of Capsular Involvement

Francesco Porpiglia[a,*], *Enrico Checcucci*[a], *Daniele Amparore*[a], *Matteo Manfredi*[a], *Federica Massa*[b], *Pietro Piazzolla*[a], *Diego Manfrin*[a], *Alberto Piana*[a], *Daniele Tota*[b], *Enrico Bollito*[b], *Cristian Fiori*[a]

[a] *Department of Urology, "San Luigi Gonzaga" Hospital, University of Turin, Orbassano, Turin, Italy;* [b] *Department of Pathology, "San Luigi Gonzaga" Hospital, University of Turin, Orbassano, Turin, Italy*

Article info

Article history:
Accepted March 26, 2019

Associate Editor:
Alexandre Mottrie

Keywords:
Three-dimensional reconstruction
Augmented reality
Hyperaccuracy three-dimensional reconstruction
Image-guided surgery
Prostatectomy
Robotics

Abstract

Background: In prostate cancer (PCa) surgical procedures, in order to maximize potency recovery, a nerve-sparing (NS) procedure is preferred. However, cancer abutting or focally extending beyond the prostate capsule increases the risk of a positive surgical margin.
Objective: To evaluate the accuracy of our new three-dimensional (3D) elastic augmented-reality (AR) system in identifying capsular involvement (CI) location of PCa during the NS phase of robot-assisted radical prostatectomy (RARP). Secondarily, the accuracy of this technology was compared with two-dimensional (2D)-based cognitive procedures.
Design, setting, and participants: A prospective study, enrolling 40 patients with PCa undergoing RARP at our center, from May to October 2018.
Surgical procedure: Patients underwent 3D AR RARP or, in case of unavailability of this technology, 2D cognitive RARP. In all patients, total anatomical reconstruction was used.
Measurements: Clinical data were collected. In order to compare the two groups, nonparametric Mann-Whitney and chi-square tests were performed. A metallic clip was placed at the level of suspicious CI on the basis of images given by the 3D AR or magnetic resonance imaging (MRI) report. The pathological analysis evaluated the presence of tumor at the level of the clip.
Results and limitations: Twenty patients were enrolled in each group. Focusing on the 3D AR group at macroscopic evaluation, the metallic clip was placed at the tumor and capsular bulging in all cases. At microscopic assessment, cancer presence was confirmed in the suspicious area in 95.4% of the cases. Moreover, CI was correctly identified in 100.0% of the cases, thanks to the 3D image overlap. These results were compared with the 2D MRI cognitive group, showing, at microscopic analysis, statistically significant

* Corresponding author. Division of Urology, Department of Oncology, School of Medicine, San Luigi Gonzaga Hospital, University of Turin, Regione Gonzole 10, 10043 Orbassano, Turin, Italy.
Tel. +39 0119026558; Fax: +39 0119038654.
E-mail address: porpiglia@libero.it (F. Porpiglia).

https://doi.org/10.1016/j.eururo.2019.03.037

superiority of the 3D AR group in CI detection during the NS phase (100% vs 47.0%; $p < 0.05$). The main limitation of this technique is that the segmentation and overlapping of the images are performed manually.
Conclusions: Our findings suggest that, with the introduction of the elastic 3D virtual models, prostate deformation is correctly simulated during surgery and lesion location is correctly identified, even in dynamic reality with a subsequent potential reduction of positive surgical margin rate and, in the meantime, maximization of functional outcomes.
Patient summary: On the basis of our findings, the three-dimensional elastic augmented-reality technology seems to help the surgeon in lesion location identification even in a dynamic phase of the intervention, optimizing the oncological outcomes.

1. Introduction

A nerve-sparing (NS) procedure is preferred to maximize the potency recovery after robot-assisted radical prostatectomy (RARP) for prostate cancer (PCa). A fine balance is required between the maximum amount of nerve fibers preserved and the risk of positive surgical margins (PSMs), considering that cancer abutting or focally extending beyond the prostate capsule increases this risk [1].

Up to now, in order to help the surgeon in intraoperative lesion identification, many experiments with molecular-imaging-guided surgery have been performed with the aim of recognizing hidden tumors, but without a clear clinical application [2].

Thus, intraoperative knowledge of the three-dimensional (3D) location of cancer lesions can prevent the surgeon from conceptualizing the procedure based on two-dimensional (2D) preoperative images, potentially reducing this risk [3].

In this setting, we already developed a professional engineer-based method to perform high-quality 3D reconstructions. The hyperaccuracy 3D reconstruction (HA3D) technology [4] allows us to create detailed 3D virtual models of the prostate that highlight the tumor and its relationship with the prostate capsule. Moreover, we already reported a preliminary experiment with augmented-reality (AR) RARP [5], proving the accuracy of images overlapping in a static phase of the intervention.

The need to identify the lesion and its relationship with the prostate capsule, mainly during the dissection phase of the intervention, has led us to further development of this technology, creating models to be superimposed even in the dynamic phase.

We specifically developed an elastic AR system based on an elastic HA3D model that simulates prostate deformation due to the grasping exercised by robotic arms during the intervention.

The aim of this study was to evaluate the accuracy of our new 3D elastic AR system in identifying capsular involvement (CI) of PCa during the NS phase of RARP. Secondarily, the accuracy of this technology was compared with a 2D-based cognitive procedure.

2. Patients and methods

2.1. Objectives

The primary endpoint was to evaluate the accuracy of our new 3D elastic AR system in identifying CI location of PCa during the NS phase of RARP.

The secondary endpoint was to compare the accuracy of this technology with 2D-based cognitive procedures.

2.2. Study population and HA3D processing

This was a prospective study, enrolling patients with PCa (clinical stages cT1–3, cN0, and cM0) whose diagnosis was based on a positive target biopsy at the index lesion [6]. All of them underwent RARP at our center, from May to October 2018. The study was conducted in accordance with good clinical practice guidelines, and informed consent was obtained from the patients. According to Italian law (Agenzia Italiana del Farmaco Guidelines for Observational Studies, March 20, 2008), no formal institutional review board or ethics committee approval was needed.

Preoperative assessment included high-resolution (1 mm slices) multiparametric magnetic resonance imaging (mp-MRI) with a 1.5-T scanner (Achieva; Philips Healthcare, Eindhoven, the Netherlands), according to a dedicated protocol, as previously described [3]. Only patients with an index lesion suspicious for CI at mp-MRI were enrolled in this study.

The images in DICOM format were processed by dedicated software, authorized for medical use by MEDICS Srl (www.medics3d.com), in order to perform HA3D reconstruction as we already described [3]. The final output was in STL format.

On the basis of the availability of this technology at our institution, the patients were scheduled for 3D elastic AR RARP or 2D cognitive RARP.

2.3. Three-dimensional elastic AR

A specific system was used to overlay virtual data on the endoscopic video displayed by a remote Da Vinci surgical console (Intuitive, Sunnyvale, CA, USA).

The HA3D virtual model of the prostate was loaded by the *pViewer* application, as we previously described [5]. This software was developed using the Unity platform [7] and C Sharp [8], and was specifically engineered to display a 3D model of the patient's prostate and to control its translation, rotation, and scale transformation values.

To improve the overlay precision, we considered prostate elasticity and deformation due to grasping and traction forces of the robotics arm during the intervention, and tried to simulate these forces with our *pViewer*.

The first challenge was addressed by approximating the deformation of the target organ by applying nonlinear parametric deformations [9] to

the 3D model meshes. Using parametric transformation formulas, it was possible to twist, bend, stretch, and taper the model. All these transformations were described along one main axis, and could be summed together in order to combine deform effects. Barr's formulas gave us fast and intuitive manipulations, with little computational effort and good visual results.

Among the available parametric deformations, we selected bend (Fig. 1) and stretch (Fig. 2) as those most suited to our visualization and overlay purposes. Since the prostate virtual model is composed of multiple meshes, in order to apply the formula uniformly to all of them, we used the method introduced by Sederberg and Parry [10].

Finally, in order to solve the issue of a realistic deformation in vivo, we opted for a human-assisted deformation by using a 3D professional mouse.

Moreover, by pressing a keyboard button, it is possible to switch the input device from using its axes for movement, rotation, and scale, to using the axes to apply forces to the hull of the parametric deformation.

Then, the video rendered by the *pViewer* application was mixed with the video taken by the endoscopic camera using a software video mixer application. The resulting stream was then sent back to the DaVinci remote console monitor in real time, where it was used by the surgeon as needed by means of the TilePro multi-input display technology.

2.4. Three-dimensional elastic AR RARP procedure

All RARP procedures were performed by a single highly experienced robotic surgeon (F.P.), according to a previously described technique [11]. The AR technology was used in four standardized key steps during the procedure, as previously reported [4].

For the purpose of the present study, the virtual image of the prostate was overlapped onto the endoscopic view using the TilePro. Our markers to guide precise manual overlapping were the prostate apex, prostate landmarks, and catheter.

The innovation in this study is that the superimposed 3D virtual model was stretched and bent according to the traction exercised on the prostate by the robotic arms, allowing dynamic chasing of prostate movement and deformation during the procedure. In order to achieve the best exposure of the tumor and suspicious CI during the NS phase of the intervention, if it was located on the anterior or anterolateral side of the prostate, the virtual model was stretched and minimally bent on the sagittal axis from front to back (Fig. 3); if the lesion was posterior or posterolateral, the model was stretched and mainly bent from back to front (Fig. 4).

Therefore, the CI location resulted in being clearly visible on the surface of the opaque 3D virtual prostate model, irrespective of its location; then, the suspicious area of CI was marked on the prostate capsule with a metallic clip (Aesculap-Braun 5 mm clips; Fig. 5).

Finally, according to presurgical indications, a partial or minimal NS procedure was carried out.

2.5. Two-dimensional cognitive procedure

As the realization of 3D models required 4–6 h of work by the bioengineers, and their presence was always required during surgery, sometimes the arrangement of 3D AR was not possible due to organizational reasons. In such cases, the patients included in this study were scheduled for 2D cognitive procedures.

Specifically for the 2D cognitive procedures, during the intervention, the surgeon had the chance of visualizing the location of the tumor and

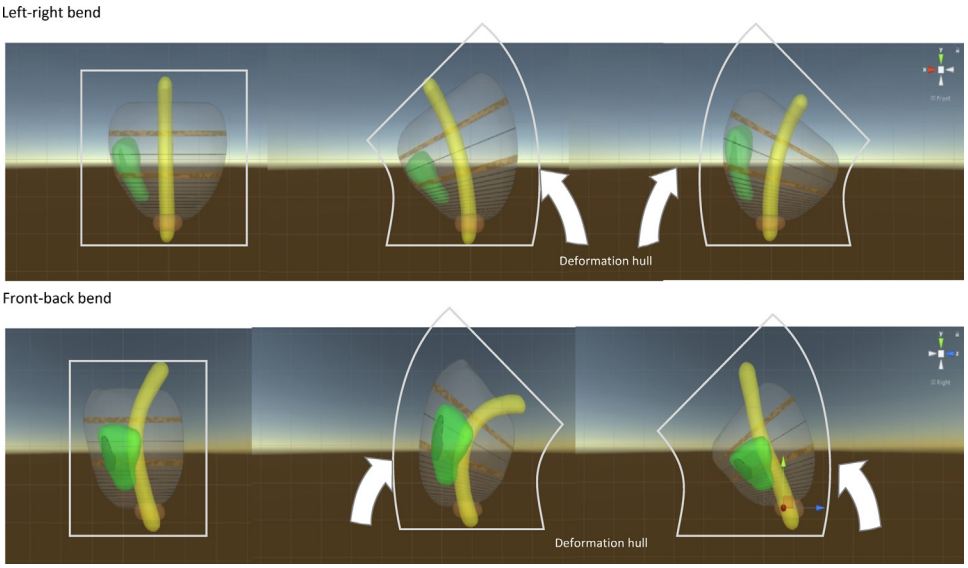

Fig. 1 – Bend deformer using global *Y* axis as the deformation main axis, along two different directions.

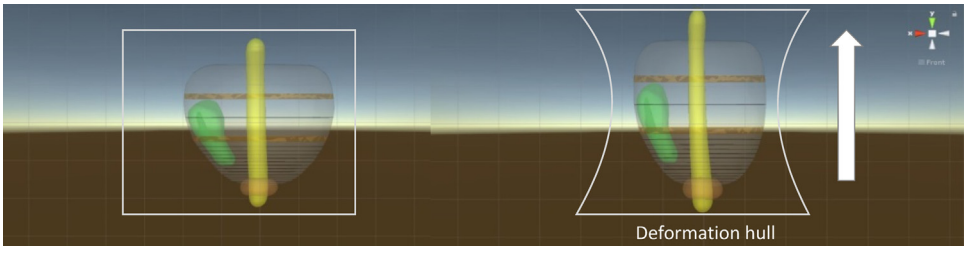

Fig. 2 – Stretch deformer using global *Y* axis as the deformation axis.

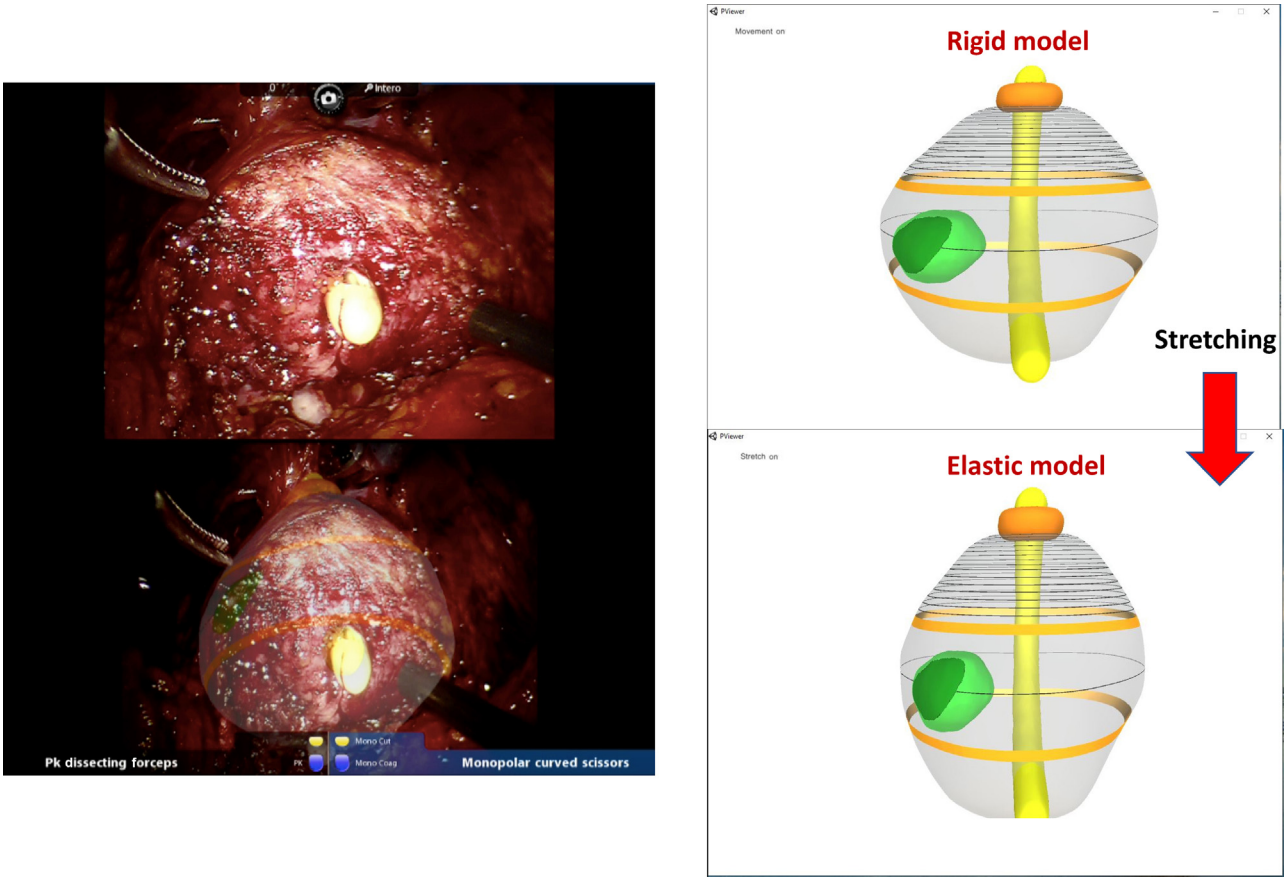

Fig. 3 – In case of posterior or anterolateral lesion, the model was mainly stretched and minimally bent.

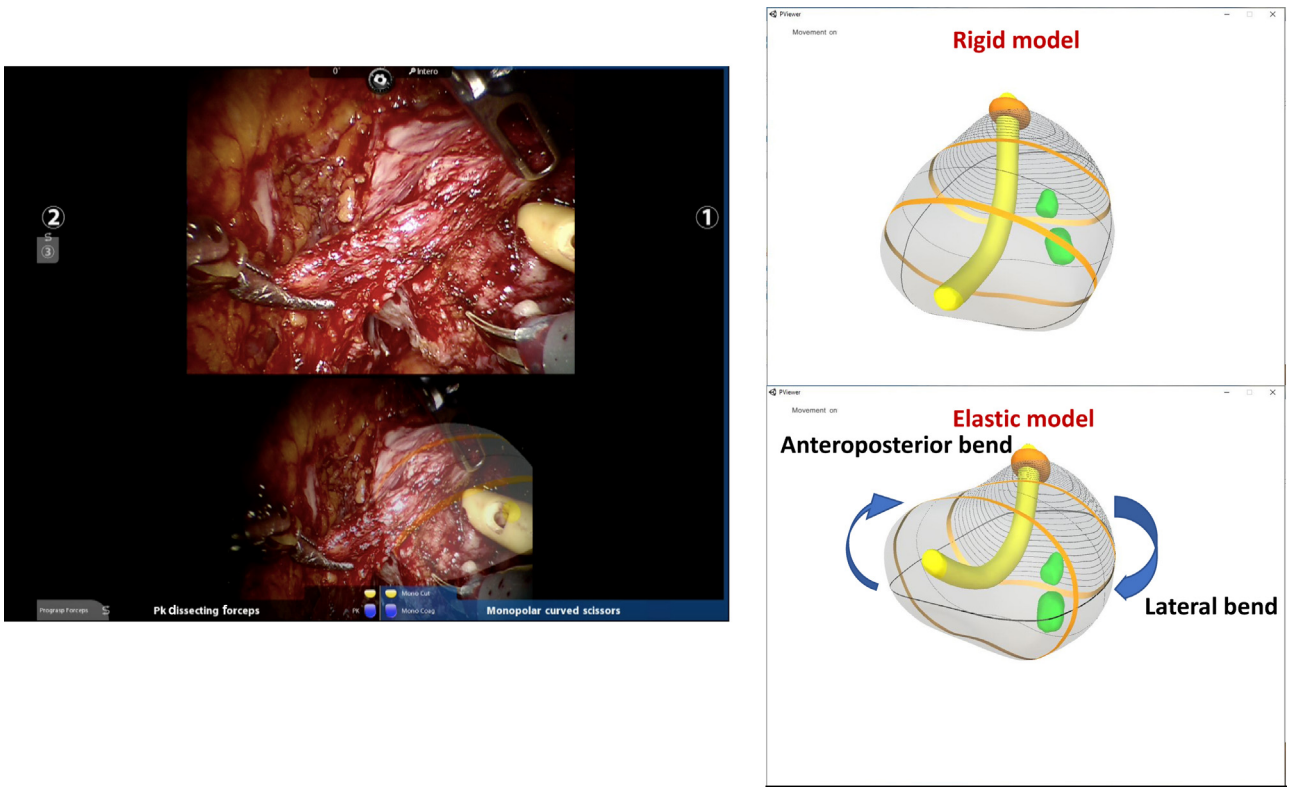

Fig. 4 – In case of posterior or posterolateral lesion, the model was stretched and mainly bent from back to front.

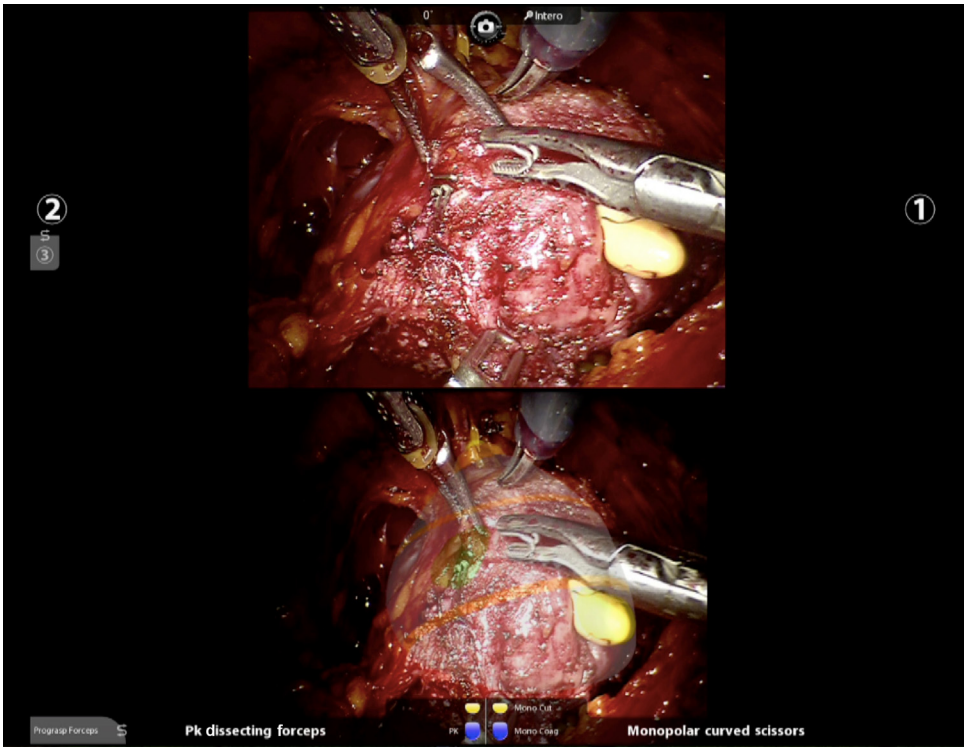

Fig. 5 – The CI location resulted in being clearly visible on the surface of the opaque 3D virtual prostate model, irrespective of its location; then, the suspicious area of CI was marked on the prostate capsule with a metallic clip. CI = capsular involvement.

CI drawn on the segmentation model used in Prostate Imaging Reporting and Data System (PI-RADS) v.2 [12].

During the dissection phase of the intervention, at the suspicious lesion and CI, as indicated by the MRI, the surgeon applied a metallic clip in order to identify the underlying tumor.

2.6. Histopathological evaluation

At histopathological evaluation, whole-mount histological sections were used as the reference standard. The prostate surface was marked with black ink, while, at the intraoperatively applied metallic clip, red and green inks were used. Then, the prostate was cut according to a previously reported method [13,14], which was modified to get 3-mm-thick sections. A first, evaluation of the presence of the tumor and bulging at the metallic clips was done during the reduction phase. Then, after a routine histological process, 5-μm sections were taken from each thick slice and stained with hematoxylin and eosin. All samples were then assessed for cancer foci by an experienced uropathology team (F.M., D.T., and E.B.). The tumor volume of each node was calculated as previously described [13]. The pathologist also assessed the pathological Gleason score [15] for each focus, and specified the presence or absence of prostatic CI as previously described [16], in particular under red and green inks.

Classification of CI was assigned according to pathological Wheeler [16].

2.7. Data analysis

Collected data included demographic variables, and for the analysis of the mp-MRI, PI-RADS v.2 classification was used to describe the lesions found [12]; location of the lesions and the presence of extracapsular extension (ECE) were recorded. Classification of CI was assigned according to radiological Wheeler [17].

Intraoperative variables, including estimated blood loss, skin-to-skin operative time, extended pelvic lymph-node dissection rate, and the numbers of full, partial, and minimal NS procedures (according to Pasadena's classification [18]) were recorded.

Postoperative variables (such as duration of catheterization and hospitalization time) and postoperative complications (graded according to Clavien-Dindo [19]), were evaluated.

Pathological variables, including classification of CI according to pathological Wheeler [16], were recorded. Specifically, for the purpose of this study, the correspondence of the metallic clip placed on the prostate capsule, with the underlying tumor location and the ECE position, was evaluated.

2.8. Statistical analysis

Means and standard deviations, and interquartile ranges were used to describe continuous variables. Categorical variables were summarized by frequency tables.

To verify the comparability between the 3D AR RARP group and the 2D cognitive RARP group, baseline variables were evaluated, testing the differences of quantitative and categorical variables with nonparametric Mann-Whitney and chi-square tests, respectively.

The inter-rater agreement for quality (categorical) items was expressed by Cohen's kappa coefficient. Data were analyzed by StatSoft v.10.

3. Results

3.1. Demographics and perioperative outcomes

Forty patients were enrolled in the present study. Twenty patients underwent 3D elastic AR RARP, whereas 20 under-

went the 2D cognitive procedure. Preoperative variables are summarized in Table 1. Multiparametric MRI revealed four (18.1%) and four (17.4%) lesions with PI-RADS ≤3, and 18 (81.8%) and 19 (82.6%) lesions with PI-RADS >3 in the 3D AR group and 2D cognitive group, respectively.

The mean lesion volume at mp-MRI was 4.4 (±2.1) cc for the 3D AR group and 4.1 (±2.4) cc for the 2D cognitive group ($p = 0.67$).

In patients who underwent 3D AR procedures, in five (22.7.0%) lesions the CI recorded at mp-MRI had a score of ≤2 according to Wheeler, while in 17 (77.2%) lesions it was ≥3F (Table 2).

In the 2D cognitive group, CI revealed a score of ≤2 according to Wheeler in seven (30.4%) lesions, while in 16 (69.6%) lesions it was ≥3F (Table 2).

Intra- and postoperative data are detailed in Table 3.

3.2. *Pathological findings*

Histopathological data are reported in Table 4.

Compared with pathological evaluation, mp-MRI correctly classified suspicious CI (Wheeler ≤L2 or ≥3L) in 19/22 (86.3%) lesions in the 3D AR group with a Cohen's kappa coefficient of 0, compared with 20/23 (86.9%) lesions in the 2D cognitive group with a Cohen's kappa coefficient of 0.72.

At pathology, the mean CI length was 5.2 (±4.4) mm in the 3D AR group and 6.0 (±5.2) mm in the 2D cognitive group ($p = 0.58$).

At macroscopic evaluation, the metallic clip was placed at the tumor in 22/22 (100%) and 20/23 (86.9%) cases in the 3D AR group and the 2D cognitive group, respectively ($p = 0.24$).

In particular, the marker was placed at suspicious capsular bulging in 22/22 (100%) and 18/23 (78.2%) cases for each group ($p = 0.06$; Fig. 6A and B).

Subsequently, microscopic assessment was performed. It confirmed cancer presence in 21/22 (95.4%) and 19/23 (82.6%) cases at the suspicious area, identified by the 3D elastic overlap and 2D cognitive template, respectively ($p = 0.37$). Moreover, CI was correctly identified in 15/15 (100.0%) cases in the 3D AR group and in eight of 17 (47.0%) cases in the 2D cognitive group ($p = 0.002$; Fig. 6C and D). Specifically for this evaluation, the sensitivity and positive predictive value were 100% (95% confidence interval) in the 3D group, whereas these were 47.1% and 100%, respectively, in the 2D group (95% confidence interval).

Finally, the AR technology reduced the risk of PSM, although the results were not statistically significant (25% vs 35%; $p = 0.73$).

4. Discussion

Recent advances in 3D reconstruction from digitalized images now make it possible to provide intraoperative surgical navigation [20–22], and different authors have reported their experiments with the use of AR during prostate surgery in laparoscopy, and anecdotally in robotics [23–25].

In order to contribute to this field, our group realized and published a preliminary experiment with AR RARP [4,26]. The innovation in that study is the software-based integration of the virtual model inside the Da Vinci robotic console (Intuitive) during robotic prostatectomy. The virtual image overlapping the endoscopic view correctly identified the tumor location in all cases [5].

However, these techniques utilized rigid prostate models. These rigid and static views do not represent the biological realism necessary to create more functional and dynamic overlapping, which may be used during the intervention.

Table 1 – Preoperative variables

Patient characteristics	Overall	3D group	Cognitive group	*p* value
Number of patients	40	20	20	
Age (yr), mean (SD)	67.2 (±5.9)	66.5 (±5.7)	67.33 (±5.9)	0.64
BMI, mean (SD)	25.89 (±3.1)	26.5 (±4.0)	26 (±3.6)	0.68
PSA (ng/ml), mean (SD)	8.9 (±5.6)	7.6 (±3.2)	9.5 (±4.6)	0.13
ASA score, median (IQR)	2 (2–3)	2 (2–3)	2 (2–3)	0.91
IPSS score, median (IQR)	7 (0–21)	7 (0–21)	8 (0–21)	0.65
IIEF-5 score, median (IQR)	21 (17–25)	22 (17–25)	22 (17–25)	0.92
GS, median (IQR)	7 (7–8)	7 (6–9)	7 (7–8)	0.88
Positive DRE, number (%)	11 (27.5)	5 (25)	6 (30)	1.0
D'Amico classification, number (%)				
Low risk	7 (17.5)	3 (13.6)	4 (18.2)	0.97
Intermediate risk	15 (37.5)	12 (54.5)	13 (59.1)	0.97
High risk	12 (30)	7 (31.8)	5 (22.7)	0.77
TNM clinical staging, number (%)				
T1	29 (72.5)	15 (75.0)	14 (70.0)	0.95
T2a	11 (27.5)	5 (25.0)	6 (30.0)	0.94
T2b	0 (0.0)	0 (0.0)	0 (0.0)	NA
T2c	0 (0.0)	0 (0.0)	0 (0.0)	NA

ASA score = American Society of Anesthesiologists score; BMI = body mass index; DRE = digital rectal examination; GS = Gleason score; IIEF = International Index of Erectile Function; IPSS = International Prostate Symptoms Score; IQR = interquartile range; NA = not available; PSA = prostate-specific antigen; SD = standard deviation; TNM = tumor-node-metastasis; 3D = three dimensional.

Table 2 – MRI characteristics

MRI characteristics	Overall	3D group	Cognitive group	*p* value
Number of lesions, mean (SD)	1.1 (±0.4)	1.1 (±0.3)	1.1 (±0.4)	1.0
Number of lesions	45	22	23	
Right lesion, number (%)	19 (42.2)	8 (36.4)	11 (47.8)	0.63
Left lesion, number (%)	22 (48.9)	14 (63.6)	8 (34.8)	0.10
Medial lesion, number (%)	4 (8.9)	0 (0.0)	4 (17.4)	0.12
Level of lesion, number (%)				
Apical	3 (6.7)	0 (0.0)	3 (13.0)	0.24
Apical-equatorial	14 (31.1)	14 (63.6)	0 (0.0)	<0.01
Equatorial	12 (26.7)	3 (13.6)	9 (39.2)	0.10
Equatorial-basal	14 (31.1)	3 (13.6)	11 (47.8)	0.03
Basal	1 (2.2)	1 (4.6)	0 (0.0)	0.97
Apical-equatorial-basal	1 (2.2)	1 (4.6)	0 (0.0)	0.97
Location of the lesion, number (%)				
Posteromedial	10 (22.2)	1 (4.5)	9 (39.1)	0.01
Posterolateral	29 (64.4)	17 (77.3)	12 (52.2)	0.14
Anterior	1 (2.2)	1 (4.5)	0 (0.0)	0.99
Anterolateral	3 (6.7)	1 (4.5)	2 (8.7)	0.97
Transitional zone	2 (4.5)	2 (9.2)	0 (0)	0.44
PI-RADS score, number (%)				
≤3	8 (17.7)	4 (18.2)	4 (17.4)	0.74
>3	37 (82.3)	18 (81.8)	19 (82.6)	0.74
Prostate volume (ml), mean	41.8 (±11.2)	47.9 (±19.7)	31.58 (±9.3)	<0.01
Lesion volume (cc), mean	4.3 (±2.3)	4.4 (±2.1)	4.1 (±2.4)	0.67
Extracapsular invasion, number (%)				
≤L2	12 (26.7)	5 (22.7)	7 (30.4)	0.80
≥L3	33 (73.3)	17 (77.3)	16 (69.6)	0.80
Seminal vesicle invasion, number (%)	5 (11.1)	3 (13.6)	2 (8.7)	0.72

L = level of prostate cancer invasion; MRI = magnetic resonance imaging; PI-RADS: Prostate Imaging Reporting and Data System; SD = standard deviation; 3D = three dimensional.

Table 3 – Intraoperative variables

Intraoperative parameters	Overall	3D group	Cognitive group	*p* value
Operative time (min), mean (SD)	128.5 (±37.7)	140.0 (±43.6)	117.5 (±42.1)	0.10
Blood loss (ml), mean (SD)	232.0 (±53.1)	240.0 (±51.6)	230 (±54.2)	0.55
Full NS, number (%)	0 (0.0)	0 (0.0)	0 (0.0)	NA
Partial NS, number (%)	24 (60)	17 (85)	7 (35.0)	<0.01
Minimal NS, number (%)	16 (40)	3 (15)	13 (65.0)	<0.01
Lymphadenectomy, number (%)	40 (100)	20 (100)	20 (100)	NA
Length of stay (d), median (IQR)	5.4 (±1.3)	5.3 (±1.8)	5.6 (±2.0)	0.62
Catheterization time (d), median (IQR)	4.6 (±1.2)	4.7 (±1.6)	4.5 (±1.9)	0.72
Postoperative complication, number (%)				
Clavien <3	3 (7.5)	1 (5.0)	2 (10.0)	1.0
Clavien ≥3	1 (2.5)	1 (5.0)	0 (0.0)	1.0
Continence recovery, number (%)				
Removal	22 (55.0)	12 (60.0)	10 (50)	0.75
1 mo	35 (87.5)	18 (90.0)	17 (85)	1.0

IQR = interquartile range; NA = not available; NS = nerve sparing; SD = standard deviation; 3D = three dimensional.

As the real prostate is composed of soft tissues that may be deformed, there is a need to obtain an elastic model. Unfortunately, in a recent review, Payan [27] reported that <10 biomechanical modeling works used in surgical practice can be found on the market.

Indeed, three main challenges should be addressed: (1) automatic generation of patient-specific models of organs and soft tissues, which can be a long and tedious task, especially when a finite element mesh has to be designed [28]; (2) in vivo estimation of patient-specific constitutive laws for such tissues [29]; and (3) real-time (or at least interactive-time) computations of these models that require fast computation of nonlinear finite elements [30].

In this scenario, we introduced our 3D elastic AR RARP using HA3D reconstruction, thanks to the application of nonlinear parametric deformations in order to approximate the deformation of the target organ. In particular, the bend deformer used the global *Y* axis as the main deformation axis, along two different directions, while the stretch deformer used the global *Y* axis alone.

In its current state, nonlinear parametric deformation allows essentially a "visual" level of accuracy, which is

Table 4 – Histopathological data

Pathological findings	Overall	3D group	Cognitive group	*p* value
Positive surgical margins, number (%)				
Overall, number (%)	12 (30.0)	5 (25.0)	7 (35)	0.73
Apex positive margins, number (%)	2 (5.0)	2 (10.0)	0 (0.0)	0.46
pT2 positive margins, number (%)	0 (0.0)	0 (0.0)	0 (0)	NA
Prostate volume (ml), mean (SD)	36.7 (15.0)	43.8 (±20.4)	26.58 (±9.2)	<0.01
Tumor volume (ml), mean (SD)	5.1 (1.9)	3.9 (±2.1)	3.35 (±1.9)	0.34
% Tumor, mean (SD)	16.1 (13.7)	12.6 (±9.0)	13.7 (8.7)	0.69
Pathological stage, number (%)				
pT2	9 (22.5)	4 (20.0)	5 (25)	1.0
pT3	31 (77.5)	16 (80.0)	15 (75.0)	1.0
Pathological GS, number (%)				
Not assessed (HT)	0 (0.0)	0 (0.0)	0 (0.0)	NA
2–6	0 (0.0)	0 (0.0)	0 (0.0)	NA
7	24 (60)	11 (55.0)	13 (65.0)	0.74
8–10	16 (40)	9 (45.0)	7 (35.0)	0.74
Extracapsular invasion, number (%)				
≤L2	11 (24.4)	5 (22.7)	6 (26.1)	0.90
≥L3	34 (75.6)	17 (77.3)	17 (73.9)	0.90

GS = Gleason score; NA = not available; SD = standard deviation; 3D = three dimensional.

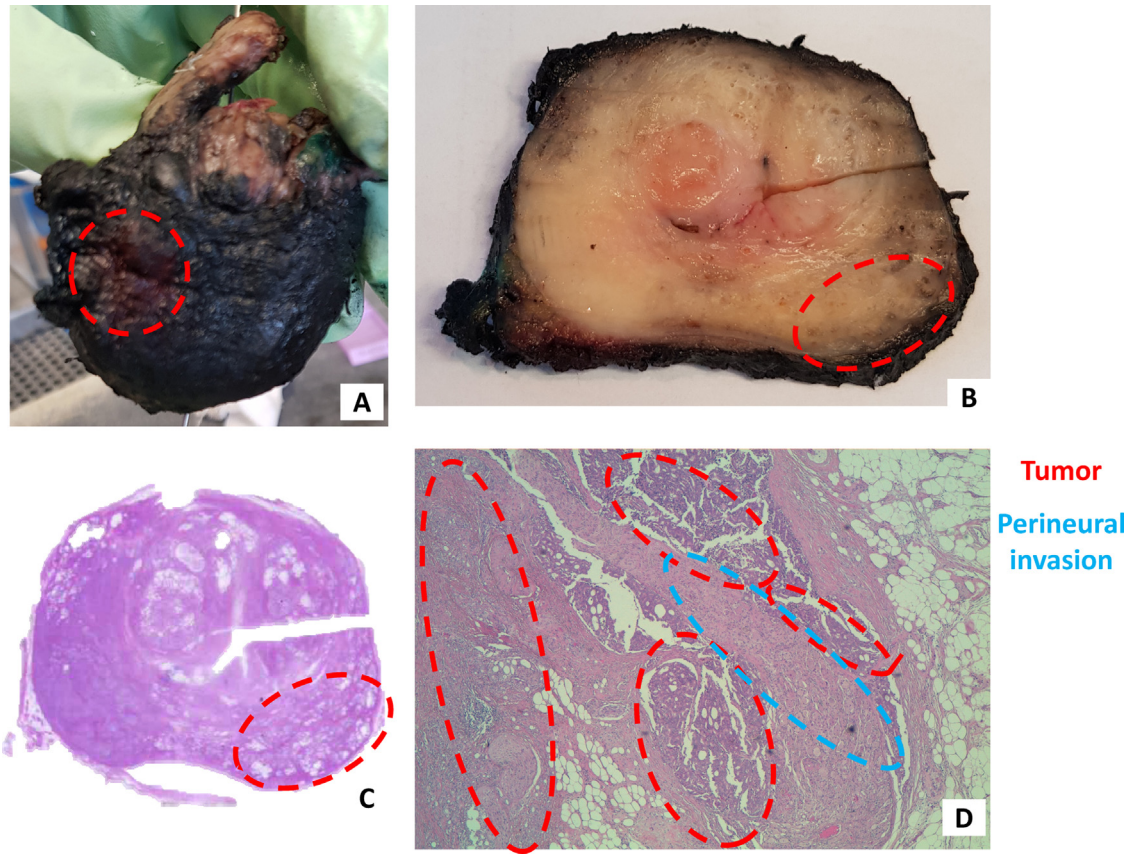

Fig. 6 – Histopathological analysis confirmed the presence of a suspicious tumor and CI at macroscopic and microscopic assessments in all the cases of the 3D AR group and in 86.9% and 47.0% of the 2D cognitive group, respectively. AR = augmented reality; CI = capsular involvement; 2D = two dimensional; 3D = three dimensional.

guaranteed by the surgeon's and assistants' experience. Mathematical evaluation of this accuracy level is currently under investigation and will be the topic of a future work.

The two deformers chosen proved to be accurate in estimating prostate deformations during surgery. In fact, notwithstanding the traction exercised on the prostate by the robotic arms, thanks to the elastic 3D overlapping model, the lesion and the CI location were dynamically identified correctly during the NS phase (100% of correct lesion identification).

We highlight that this great precision was achieved even when the mean length of CI was only 5.2 (±4.4) mm, and the CI had spike morphology in 86.6% of the lesions.

These findings suggest that the accuracy offered by this technology could allow for "real-time" intraoperative tailoring of the robotic procedure to the specific anatomy of the patient and the specific location of the cancer.

For the first time ever, our 3D AR system was used in a dynamic phase of the intervention. This new elastic technology allowed us to dynamically chase prostate movement and deformation during the NS phase.

Focusing on a comparison with the 2D cognitive group, in this study it was discovered that the location of the suspicious lesion on the basis of the 2D images required a hard mental imagination process, and the accuracy of lesion identification was poorer. In fact, in the 2D cognitive group, where the procedures were performed only on the basis of MRI reports, the metallic clip location corresponded to CI in 47% of cases with a statistically significant negative difference, compared with the 3D AR group ($p = 0.002$). Nevertheless, we emphasize that these results might have been affected by the possibly underpowered sample size.

This greater effort in perceiving the three dimensionality of the organ, and therefore the correct localization on the three spatial planes of the lesion, resulted in a greater number of PSMs in the group of patients who underwent cognitive procedures (25.0% vs 35.0%).

Even when not statistically significant, this trend, increasing the sample size, could lead to a potential oncological and functional benefit for patients.

It would be useful, particularly in the case of negative ECE on mp-MRI, to perform a full NS RARP and simultaneously selectively manage the neurovascular bundles (NVBs). For example, the neurovascular tissue could be resected more widely at the suspicious lesion only, in order to reduce the PSM rate.

In case of locally advanced disease (positive ECE), the NVBs could be preserved except at the suspicious ECE, where a wider resection guided by superimposed 3D virtual imaging could facilitate oncological safety.

This greater preservation of NVBs without compromising oncological safety could permit maximization of functional outcomes even in cohorts of patients with locally advanced tumors.

Moreover, it is interesting to note that the NS approach was more conservative in the 3D group than in the 2D group, even when both clinical and pathological features of PCa were similar. As we already demonstrated in our previously published paper [3], visualization of the 3D models allowed the surgeon to have a better understanding of the disease. Hence, the surgeon was more confident and "braver" in performing the NS.

We think that this new implementation of the robotic platform can represent a new paradigm of the treatment of PCa in the "precision surgery" era [31]. The procedures can be tridimensionally modulated in real time on the basis of a patient's specific anatomy and, in particular, CI location.

It could especially be useful for the beginner surgeon; the possibility of having real-time visualization of tumor location and CI location permits safer NS performance.

Moreover, particularly in patients with high-risk PCa, where oncological outcomes are even more important, independent of the degree of NS, this technology could be particularly useful to reduce the risk of PSMs.

Finally, we underline that this new technology, based on AR images, has been of increased interest not only in prostate surgery but also in robotic partial nephrectomy, especially during the resection of totally endophytic and posteriorly located renal masses. The introduction of specifically developed nonlinear parametric deformations can allow simulation of kidney movement during the surgery, and therefore a precise overlap of the images that help the surgeon during lesion margin identification [32].

The current study is not devoid of limitations. First of all, it is important to note that HA3D reconstruction was based on mp-MRI images, and the presence of CI was evaluated with this tool that, historically, accurately identified the CI, in the range from 30% to 60%. However, in our institution, we had expert MRI readers that obtained higher ECE identification (area under the curve 0.72–0.74) [33]. Hence, we can state that the information obtained from CI at MRI was effective.

Second, segmentation of prostate tumors was performed manually; an experienced urologist and an experienced radiologist were necessary to complete the segmentation process.

Third, the entire overlap process is operator dependent, because the 3D mouse needs to be manipulated by an assistant during the procedure, to allow for proper orientation and deformation of the 3D model. The next evolution of the technology would be an automated model consolidated to organ movements during the surgery. Moreover, access to more computationally complex techniques, such as those that simulate tissue dynamics, will allow the quality and realism of the deformations to improve. Finally, as previously stated, the comparison between the groups might have been less reliable due to the small sample size.

5. Conclusions

Our findings suggest that, with the introduction of the elastic 3D virtual models, prostate deformation is correctly simulated during surgery, and lesion location is correctly identified, even in dynamic reality.

This new technology allowed us to perform a 3D elastic AR RARP, optimizing the NS tailoring with a subsequent potential reduction of PSM rate and, in the meantime, possible maximization of the functional outcomes.

Further research is required to corroborate these early encouraging findings, and a prospective randomized study is needed to verify the real clinical advantages of 3D AR image-guided surgery.

Author contributions: Francesco Porpiglia had full access to all the data in the study and takes responsibility for the integrity of the data and the accuracy of the data analysis.

Study concept and design: Porpiglia.
Acquisition of data: Piana, Massa, Tota.
Analysis and interpretation of data: Bollito, Checcucci, Amparore.
Drafting of the manuscript: Checcucci, Amparore.
Critical revision of the manuscript for important intellectual content: Fiori, Manfredi.
Statistical analysis: Checcucci, Piana.
Obtaining funding: None.
Administrative, technical, or material support: Piazzolla, Manfrin.
Supervision: Porpiglia, Fiori.
Other: None.

Financial disclosures: Francesco Porpiglia certifies that all conflicts of interest, including specific financial interests and relationships and affiliations relevant to the subject matter or materials discussed in the manuscript (eg, employment/affiliation, grants or funding, consultancies, honoraria, stock ownership or options, expert testimony, royalties, or patents filed, received, or pending), are the following: None.

Funding/Support and role of the sponsor: None.

Appendix A. Supplementary data

The Surgery in Motion video accompanying this article can be found in the online version at https://doi.org/10.1016/j.eururo.2019.03.037 and via www.europeanurology.com.

References

[1] Alchin DR, Murphy D, Lawrentschuk N. Predicting the risk of positive surgical margins following robotic-assisted radical prostatectomy. Minerva Urol Nefrol 2017;69:56–62.
[2] Boustani AM, Pucar D, Saperstein L. Molecular imaging of prostate cancer. Br J Radiol 2018;91:20170736.
[3] Porpiglia F, Bertolo R, Checcucci E, et al. Development and validation of 3D printed virtual models for robot-assisted radical prostatectomy and partial nephrectomy: urologists' and patients' perception. World J Urol 2018;36:201–7.
[4] Porpiglia F, Fiori C, Checcucci E, Amparore D, Bertolo R. Augmented reality robot-assisted radical prostatectomy: preliminary experience. Urology 2018;115:184.
[5] Porpiglia F, Checcucci E, Amparore D, et al. Augmented-reality robot-assisted radical prostatectomy using hyper-accuracy three-dimensional reconstruction (HA3D™) technology: a radiological and pathological study. BJU Int. In press. https://doi.org/10.1111/bju.14549.
[6] Ahmed HU. The index lesion and the origin of prostate cancer. N Engl J Med 2009;361:1704–6.
[7] Unity. https://unity3d.com/.
[8] Microsoft. https://docs.microsoft.com/en-us/dotnet/csharp/language-reference/language-specification/.
[9] Barr AH. Global and local deformations of solid primitives. SIGGRAPH Comput Graph 1984;18:21–30.
[10] Sederberg TW, Parry SR. Free-form deformation of solid geometric models. SIGGRAPH Comput Graph 1986;20:151–60.
[11] Porpiglia F, Bertolo R, Manfredi M, et al. Total anatomical reconstruction during robot-assisted radical prostatectomy: implications on early recovery of urinary continence. Eur Urol 2016;69:485–95.
[12] Weinreb JC, Barentsz JO, Choyke PL, et al. PI-RADS Prostate Imaging – Reporting and Data System: 2015, version 2. Eur Urol 2016;69:16–40.
[13] Montironi R, Lopez-Beltran A, Mazzucchelli R, Scarpelli M, Bollito E. Assessment of radical prostatectomy specimens and diagnostic reporting of pathological findings. Pathologica 2001;93:226–32.
[14] Varma M, Morgan JM. The weight of the prostate gland is an excellent surrogate for gland volume. Histopathology 2010;57:55–8.
[15] Epstein JI, Egevad L, Amin MB, Delahunt B, Srigley JR, Humphrey PA. The 2014 International Society of Urological Pathology (ISUP) consensus conference on Gleason grading of prostatic carcinoma: definition of grading patterns and proposal for a new grading system. Am J Surg Pathol 2016;40:244–52.
[16] Wheeler TM, Dillioglugil O, Kattan MW, et al. Clinical and pathological significance of the level and extent of capsular invasion in clinical stage T1-2 prostate cancer. Hum Pathol 1998;29:856–62.
[17] Porpiglia F, Manfredi M, Mele F, et al. Preoperative multi-parametric prostate magnetic resonance imaging to predict capsular invasion prior to robot-assisted radical prostatectomy—our experience after 400 cases. Eur Urol Suppl 2016;15:269.
[18] Montorsi F, Wilson TG, Rosen RC, et al. Best practices in robot-assisted radical prostatectomy: recommendations of the Pasadena Consensus Panel. Eur Urol 2012;62:368–81.
[19] Dindo D, Demartines N, Clavien PA. Classification of surgical complications: a new proposal with evaluation in a cohort of 6336 patients and results of a survey. Ann Surg 2004;240:205–13.
[20] Bernhardt S, Nicolau SA, Soler L, Doignon C. The status of augmented reality in laparoscopic surgery as of 2016. Med Image Anal 2017;37:66–90. http://dx.doi.org/10.1016/j.media.2017.01.007.
[21] Manfredi M, Mele F, Garrou D, et al. Multiparametric prostate MRI: technical conduct, standardized report and clinical use. Minerva Urol Nefrol 2018;70:9–21.
[22] Jo JK, Hong SK, Byun SS, Zargar H, Autorino R, Lee SE. Positive surgical margin in robot-assisted radical prostatectomy: correlation with pathology findings and risk of biochemical recurrence. Minerva Urol Nefrol 2017;69:493–500.
[23] Ukimura O, Gill IS. Image-fusion, augmented reality, and predictive surgical navigation. Urol Clin North Am 2009;36:115–23.
[24] Simpfendörfer T, Baumhauer M, Müller M, et al. Augmented reality visualization during laparoscopic radical prostatectomy. J Endourol 2011;25:1841–5.
[25] Cohen D, Mayer E, Chen D, et al. Prostate cancer imagingComputer-aided diagnosis, prognosis, and intervention, augmented reality image guidance in minimally invasive prostatectomy. Berlin, Heidelberg, Germany: Springer; 2010. p. 101–10.
[26] Porpiglia F, Bertolo R, Amparore D, et al. Augmented reality during robot-assisted radical prostatectomy: expert robotic surgeons' on-the-spot insights after live surgery. Minerva Urol Nefrol 2018;70:226–9.
[27] Payan Y. Soft tissue biomechanical modeling for computer assisted surgery. Berlin, Heidelberg, Germany: Springer; 2012.
[28] Bucki M, Lobos C, Payan Y. A fast and robust patient specific finite element mesh registration technique: application to 60 clinical cases. Med Image Anal 2010;14:303–17.
[29] Schiavone P, Promayon E, Payan Y. Lecture notes in computer science, 5958. Springer; 2010. p. 1–10.
[30] Gonzalez D, Cueto E, Chinesta F. Computational patient avatars for surgery planning. Ann Biomed Eng 2016;44:35–45.
[31] Autorino R, Porpiglia F, Dasgupta P, et al. Precision surgery and genitourinary cancers. Eur J Surg Oncol 2017;43:893–908.
[32] Porpiglia F, Checcucci E, Amparore D, et al. 3D Elastic augmented reality robot assisted partial nephrectomy for central and posterior renal masses: a new tool for a better resection of the tumor. Eur Urol Suppl 2019;18:e2276.
[33] Russo F, Manfredi M, Panebianco V, et al. Radiological Wheeler staging system: a retrospective cohort analysis to improve the local staging of prostate cancer with multiparametric magnetic resonance imaging. Minerva Urol Nefrol. In press. https://doi.org/10.23736/S0393-2249.19.03248-X.